

UPCommons

Portal del coneixement obert de la UPC

<http://upcommons.upc.edu/e-prints>

Ferrer, A.; Giusti, S. Inverse homogenization using the topological derivative.
"Engineering computations", 28 Setembre 2021, p. 1-21.
DOI: < <https://doi.org/10.1108/EC-08-2021-0435>>.

© 2021, Emerald Publishing Limited. This AAM is provided for your own personal use only. It may not be used for resale, reprinting, systematic distribution, emailing, or for any other commercial purpose without the permission of the publisher.

INVERSE HOMOGENIZATION USING THE TOPOLOGICAL DERIVATIVE

ABSTRACT. Purpose: Solve the inverse homogenization problem, or so-called material design problem, using the topological derivative concept.

Methodology: The optimal topology is obtained through a relaxed formulation of the problem by replacing the characteristic function with a continuous design variable, so-called density variable. The constitutive tensor is then parametrized with the density variable through an analytical interpolation scheme that is based on the topological derivative concept. The intermediate values that may appear in the optimal topologies are removed by penalizing the Perimeter functional.

Findings: The proposed methodology allow us to use the topological derivative concept for solving the inverse homogenization problem and to fulfil the optimality conditions of the problem with the use of classical optimization algorithms. We solved several material design examples through a projected gradient algorithm to show the advantages of the proposed method.

Originality: The material design problem based on the topological derivative concept is solved in a continuous optimization framework. The optimization process benefits from the intermediate values that provide the proposed method reaching solutions that the topological derivative had not been able to find before. In addition, the presented theory opens the path to propose a new framework of research where the topological derivative uses classical optimization algorithms.

1. INTRODUCTION

The aim of this work is to solve the inverse homogenization problem, hereinafter also called material design problem, which consists in finding the optimal topology of a microstructure whose effective constitutive response, so-called \mathbb{C}^h , is identical to a pre-established behavior \mathbb{C}^* .

The concept of inverse homogenization was first presented in [Sigmund, 1994, Sigmund, 1995] by Sigmund and their co-workers in the '90s. The authors proposed to use as design variables the distribution of the density of a reference structural material in the base cell and consider classical optimization algorithms. The constitutive tensor is then parametrized with the the density variable through an auto-penalized analytical interpolation (SIMP method). The optimality conditions for this approach are the classical ones for a continuous-parametric problem. See, for instance, the book of [Bendsøe and Sigmund, 2003] and the bibliography cited therein related to this topic.

Another approach to solve this problem is based on the concept of topological derivatives [Novotny and Sokolowski, 2013]. Typically, this approach considers a level-set function for the geometrical description of the material distribution and

Date: 2021.

Key words and phrases. Synthesis of materials, Topology optimization, Material design, inverse homogenization, architected materials, relaxed formulation, SIMP-ALL.

proposes a fixed-point algorithm for reaching the optimality condition of considering topological changes, see for example [Amstutz et al., 2010, Giusti and Novotny, 2016]. The optimality condition could be hard to accomplish depending on the shape functional and the numerical discretization that is considered, specially on the interface. Different works to improve the discretization on the interface may be found in [Ferrer, 2017, Amstutz et al., 2018] and more recently in [Vermaak et al., 2019].

Recently, in [Ferrer, 2019], the topological derivative has succeeded to solve topology optimization problems through a relaxed formulation. This approach proposed on an isotropic interpolation, such as SIMP methodologies, such that the derivative in the void and material part of the domain coincides with the topological derivative. This interpolation function is called SIMP-ALL. In addition, the SIMP-ALL interpolation has been proved in [Ferrer, 2019] to remain in between the HS bounds ensuring that the intermediate values that may appear can always be interpreted as the homogenization of some micro-structures. The main property of the approach is that the sensitivity of the shape-function when a topological change is considered now becomes a continuous change and therefore continuous optimization algorithms become available.

To avoid the problem of the possible existence of intermediate values for the material properties in this relaxed formulation, a perimeter functional is also added to the optimization procedure. The perimeter functional is usually added in topology optimization for ensuring existence of optimal topologies [Allaire, 2012]. Although different methods exists for computing the perimeter, we follow in this work the approach proposed in [Amstutz and Van Goethem, 2012]. The perimeter functional will remedy the main disadvantage of the relaxed formulation (intermediate values in the optimal topology) and will ensure the manufacturability of the optimal topologies. In addition, in this work, we opt for square microstructure domains for simplicity. However, the shape of the microstructure boundary can also be used as a design variable of the problem (rectangle, hexagon, etc). See work [Podestá et al., 2019] for further details.

This paper is organized as follows. In Section 2, the material design problem is briefly introduced together with the topological derivative of the elastic constitutive tensor. Section 3 explains the main concepts on the use of the topological derivative of the constitutive tensor in the material design framework. Two kinds of methods are presented here. The capabilities of each one to solve the inverse homogenization problem are discussed. The notions of perimeter functional and the closed-form for the computation of the gradient are introduced in Section 4. The material design problem is reformulated here to consider the minimization of the perimeter and manufacturability conditions. Its advantages and disadvantages are also discussed. Finally, several numerical examples are carried out in Section 5 while the main conclusions of this work are provided in Section 6.

2. SETTING OF MATERIAL DESIGN PROBLEM

2.1. Formulation of the problem. Consider the unit cube $Y = (0, 1)^N$, with $N = 2$, then the cell problem or microstructure problem can be written as solving for the indices $1 < i, j < N$ the following equation:

$$\begin{cases} -\operatorname{div}(\mathbb{C} : (e_{ij} + \varepsilon(w_{ij}))) = 0 & \text{in } Y, \\ y \mapsto w_{ij}(y) & Y - \text{periodic}, \end{cases} \quad (1)$$

where the tensor $e_{ij} = \frac{1}{2}(e_i \otimes e_j + e_j \otimes e_i)$ is one element of the canonical basis of symmetric matrices, $\varepsilon(\cdot)$ is the symmetric part of the gradient of (\cdot) and \mathbb{C} is the fourth-order elasticity tensor. The solution w_{ij} is called the corrector function or fluctuation field. In practice, this problem have to be solved three times (for $N = 2$): $e_{11} = e_1 \otimes e_1$, $e_2 \otimes e_2$ and $e_{12} = \frac{1}{2}(e_1 \otimes e_2 + e_1 \otimes e_2)$.

To give a mathematically precise meaning to (1), let us introduce the subspace $\mathcal{V} = H_{\#}^1(Y; \mathbb{R}^N)$ of all functions $u \in H^1(Y; \mathbb{R}^N)$ which are periodic, i.e., with traces equal on opposite sides of the unit cell Y . The cell problem admits the following weak form: for given indices $1 < i, j < N$ find $w_{ij} \in \mathcal{V}$ such that

$$\int_Y \varepsilon(w_{ij}) : \mathbb{C} : \varepsilon(\phi) + \int_Y e_{ij} : \mathbb{C} : \varepsilon(\phi) = 0 \quad \forall \phi \in \mathcal{V}, \quad (2)$$

which admits a unique solution up to a rigid body motion. By introducing the dual paring notation $(e_1, \mathbb{C} : e_2) = \frac{1}{|Y|} \int_Y e_1 : \mathbb{C} : e_2$ and dividing by $|Y|$ equation (2), we can write the cell problem as find for the indices $1 < i, j < N$ the correctors w_{ij} solution of

$$(\varepsilon(\phi), \mathbb{C} : \varepsilon(w_{ij})) + (\varepsilon(\phi), \mathbb{C} : e_{ij}) = 0 \quad \forall \phi \in \mathcal{V}. \quad (3)$$

Following this notation, the correctors yield an explicit formula for the homogenized constitutive tensor which reads as

$$\mathbb{C}_{ijkl}^h = (e_{ij}, \mathbb{C} : e_{kl}) + (e_{ij}, \mathbb{C} : \varepsilon(w_{kl})), \quad (4)$$

or equivalently, using the weak form (3),

$$\mathbb{C}_{ijkl}^h = (e_{ij} + \varepsilon(w_{ij}), \mathbb{C} : (e_{kl} + \varepsilon(w_{kl}))). \quad (5)$$

2.2. Topological derivative of the elastic constitutive tensor. For the sensitivity of the elastic constitutive tensor, we consider two materials: the base material \mathbb{C}_1 and the weak material (or void material) \mathbb{C}_0 . Both tensors can be written as:

$$\begin{aligned} \mathbb{C}_0 &= 2\mu_0 \mathbb{I} + (\kappa_0 - \mu_0) (I \otimes I), \\ \mathbb{C}_1 &= 2\mu_1 \mathbb{I} + (\kappa_1 - \mu_1) (I \otimes I), \end{aligned} \quad (6)$$

being μ_i and κ_i (for $i = 0, 1$) the Lamé coefficients for both material phases. Let us consider the fixed cell domain Y that is split in Y_0 and Y_1 . For the indices $1 < i, j, k, l < N$, the topological gradient $\mathcal{T}_D \mathbb{C}^h$ evaluated at each point $\hat{y} \in Y$ are given by:

$$(\mathcal{T}_D \mathbb{C}^h)_{ijkl} = \begin{cases} (\mathcal{T}_D \mathbb{C}_0^h)_{ijkl} = [e_{ij} + e(w_{ij})] : d\mathbb{C}_0 : [e_{kl} + e(w_{kl})] & \forall \hat{y} \in Y_0, \\ (\mathcal{T}_D \mathbb{C}_1^h)_{ijkl} = [e_{ij} + e(w_{ij})] : d\mathbb{C}_1 : [e_{kl} + e(w_{kl})] & \forall \hat{y} \in Y_1, \end{cases} \quad (7)$$

where w_{ij} are the correctors functions solution of problem (3). The polarization tensors $d\mathbb{C}_0$ and $d\mathbb{C}_1$ are:

$$\begin{aligned} d\mathbb{C}_0 &= 2\mu_0 (\mu_1 - \mu_0) q_{\mu_0} \mathbb{I} + [\kappa_0 (\kappa_1 - \kappa_0) q_{\kappa_0} - \mu_0 (\mu_1 - \mu_0) q_{\mu_0}] (I \otimes I), \\ d\mathbb{C}_1 &= 2\mu_1 (\mu_0 - \mu_1) q_{\mu_1} \mathbb{I} + [\kappa_1 (\kappa_0 - \kappa_1) q_{\kappa_1} - \mu_1 (\mu_0 - \mu_1) q_{\mu_1}] (I \otimes I), \end{aligned} \quad (8)$$

with

$$\begin{aligned} q_{\mu_1} &= q(\mu_1, \mu_0, \eta_{\mu_1}), q_{\kappa_1} = q(\kappa_1, \kappa_0, \eta_{\kappa_1}), \eta_{\mu_1} = \frac{\kappa_1 \mu_1}{2\mu_1 + \kappa_1} \text{ and } \eta_{\kappa_1} = \mu_1; \\ q_{\mu_0} &= q(\mu_0, \mu_1, \eta_{\mu_0}), q_{\kappa_0} = q(\kappa_0, \kappa_1, \eta_{\kappa_0}), \eta_{\mu_0} = \frac{\kappa_0 \mu_0}{2\mu_0 + \kappa_0}, \text{ and } \eta_{\kappa_0} = \mu_0 \end{aligned} \quad (9)$$

where $q(t_1, t_2, t_3) = \frac{(t_1 + t_3)}{t_1(t_2 + t_3)}$. The proof of the previously presented results can be found in [Amstutz et al., 2010, Ferrer, 2019].

3. USE OF TOPOLOGICAL DERIVATIVE IN MATERIAL DESIGN

3.1. **Using topological derivative within level-set formulation.** The topological derivative has been commonly used in topology optimization in combination with a level-set description of the domain. The first successful algorithm was proposed in [Amstutz and Andrä, 2006] and used for material design in [Amstutz et al., 2010]. We briefly recall this approach in this work. By defining a characteristic function $\chi \in L^\infty_{\#}(Y, \{0, 1\})$ in the space of $L^\infty(Y, \{0, 1\})$ functions with periodic conditions such that

$$\chi(y) = \begin{cases} 0 & \text{if } y \in Y_0 \\ 1 & \text{if } y \in Y_1 \end{cases}, \quad (10)$$

the elasticity tensor $\mathbb{C}(\chi)$, to be used in cell problem (2), can be constructed as:

$$\mathbb{C}(\chi) = (1 - \chi)\mathbb{C}_0 + \chi\mathbb{C}_1. \quad (11)$$

The two parts of the domain are described by the positive or negative part of the level-set function $\Psi \in L^2(Y)$. This is

$$Y_0 = \{y \in Y, \Psi(y) < 0\}, \text{ and } Y_1 = \{y \in Y, \Psi(y) > 0\}. \quad (12)$$

Now, let us consider the topological derivative $T_D\mathcal{F}_\chi$ of a general functional \mathcal{F}_χ . According to [Amstutz and Andrä, 2006], a sufficient condition of *local optimality* of minimization problems for the class of perturbations consisting of circular inclusions is

$$T_D\mathcal{F}_\chi(y) > 0 \quad \forall y \in Y. \quad (13)$$

To devise a level-set-based algorithm whose aim is to produce a topology that satisfies (13), it is convenient to define the function

$$g(y) = \begin{cases} -T_D\mathcal{F}_\chi(y) & \text{if } y \in Y_0 \\ T_D\mathcal{F}_\chi(y) & \text{if } y \in Y_1 \end{cases}. \quad (14)$$

With the above definition, it can be easily established that the sufficient condition (13) is satisfied if the following equivalence relation between the functions g and the level-set Ψ holds

$$\exists \tau > 0 \quad \text{s.t.} \quad g = \tau \Psi, \quad (15)$$

or, equivalently,

$$\theta := \arccos \left[\frac{\langle g, \Psi \rangle_{L^2(Y)}}{\|g\|_{L^2(Y)} \|\Psi\|_{L^2(Y)}} \right] = 0, \quad (16)$$

where θ is the angle between the vectors g and Ψ in $L^2(Y)$. Therefore, the above condition indicates that at the optimum the functions g and Ψ must be parallel in the functional space.

3.1.1. *General optimization procedure.* Starting from a given level-set function $\Psi_0 \in L^2(Y)$ which defines the chosen initial guess for the optimum topology, the algorithm proposed by [Amstutz and Andrä, 2006] produces a sequence $(\Psi_i)_{i \in \mathbb{N}}$ of level-set functions that provides successive approximations to the sufficient condition for optimality (15). The sequence satisfies

$$\begin{aligned} \Psi_0 &\in L^2(Y), \\ \Psi_{i+1} &\in \text{co}(\Psi_i, g_i) \quad \forall i \in \mathbb{N}, \end{aligned} \quad (17)$$

where $\text{co}(\Psi_i, g_i)$ is the convex hull of $\{\Psi_i, g_i\}$. In the current procedure the initial guess Ψ_0 is normalized. With \mathcal{S} denoting the unit sphere in $L^2(Y)$, the algorithm is explicitly given by

$$\begin{aligned} \Psi_0 &\in \mathcal{S}, \\ \Psi_{i+1} &= \frac{1}{\sin \theta_i} \left[\sin((1 - k_i)\theta_i)\Psi_i + \sin(k_i\theta_i)\frac{g_i}{\|g_i\|_{L^2(Y)}} \right], \end{aligned} \quad (18)$$

where $k_i \in [0, 1]$ is a step size determined by a line-search in order to decrease the value of the cost functional \mathcal{F}_χ . The iterative process is stopped when for some iteration the obtained decrease in \mathcal{F}_χ is smaller than a given numerical tolerance. If, at this stage, the optimality condition (15,16) is not satisfied to the desired degree of accuracy, i.e. if $\theta_{i+1} > \epsilon_\theta$, where ϵ_θ is a pre-specified convergence tolerance, then a uniform mesh refinement of the structure is carried out and the procedure is continued. For more details see [Amstutz and Andrä, 2006].

3.1.2. *Optimization problem.* The material design problem can be formulated as

$$\min_{\chi \in L^\infty_\#(Y)} \mathcal{F}_\chi = \|\mathbb{C}^h(\chi) - \mathbb{C}^*\|_2, \quad (19)$$

where \mathbb{C}^h corresponds to the homogenized constitutive tensor introduced in (5) and \mathbb{C}^* is a target constitutive tensor representing a desired behaviour of the cell Y at macroscopic level. In the above problem the design variable is the characteristic function χ , whose relation with the level-set function Ψ is given by expressions (10) and (12). According to [Giusti et al., 2010] and by a simple chain rule procedure, the associated topological derivative of the above functional is given by,

$$\mathcal{T}_D \mathcal{F}_\chi = \mathcal{F}_\chi^{-1}(\mathbb{C}^h(\chi) - \mathbb{C}^*) \cdot \mathcal{T}_D \mathbb{C}^h \quad (20)$$

where $\mathcal{T}_D \mathbb{C}^h$ is defined in (7). Preliminary result of this class of functional together with the topological derivative (20) was presented in [Giusti et al., 2010], and for a further and detailed analysis and applications of the technique can be found in [Méndez et al., 2017, Podestá et al., 2019, R.Yera et al., 2020, Rossi et al., 2021].

Note that the problem stated in (19) has a global solution (global minimum) when $\mathbb{C}^h(\chi)$ reaches \mathbb{C}^* . Therefore, in this topological configuration, the topological derivative (20) vanishes. At this point, the local optimality condition (13) of the optimization procedure based on level-set geometrical description, fails. Equivalently, the parallelism of any vector Ψ with zero is not possible to measure, see (15). From a numerical point of view, this kind of procedure tends to provide very oscillatory level-set function since at the same time is trying to fulfill the unitary norm condition and the parallelism condition with zero. Thus, a different method should be proposed to remedy this major inconvenient.

3.2. **Using topological derivative with in a relaxed formulation.** An alternative to level-set methods is considering a relaxed formulation of the problem where the topology $\chi \in L^\infty(Y, \{0, 1\})$ is replaced in this case by a density function $\rho \in \mathcal{R} = L^\infty_\#(Y, [0, 1])$. The main advantage is that the problem becomes differentiable and thus classical continuous optimization algorithms are available. The main disadvantage is that the value of the elastic properties in gray areas should be provided.

Regarding this relation, one possibility is to use the homogenization theory for a family of parametrized microstructures. The inconvenience is that this process is computationally expensive since the cell problem should be solved for as many microstructures to characterize the parametric domain. See for example [Ferrer et al., 2021].

Another option is to use an analytic isotropic relation. One well-known example is the SIMP method, where the homogenized constitutive tensor is heuristically proposed as follows $\mathbb{C}(\rho) = (1 - \rho^p)\mathbb{C}_0 + \rho^p\mathbb{C}_1$ where \mathbb{C}_0 and \mathbb{C}_1 stands for the void and material constitutive tensors. The advantage of this approach is that the relation $\mathbb{C}(\rho)$ is analytic and no homogenization process is needed. However, the first disadvantage is that the value p is not clear and depends on the problem to solve. Taking $p = 3$ is usually an appropriate choice. However, in complex examples, the exponent p should be increased in order to obtain clear interfaces of the domain. In addition, high values of p significantly deteriorate the condition of the optimization problem. Even more worrisome, if intermediate values remain in the final topology, there is no guarantee that they can be understood as a homogenization of a microstructure. The connection of SIMP-like methods and topological derivative is analyzed and analytically determined in [Amstutz, 2011b].

As an alternative, we can use the SIMP-ALL interpolation [Ferrer, 2019] method which is also an isotropic interpolation. The advantages are that no exponent parameter p is required in the interpolation and additionally, the interpolation lies in between the HS bounds regardless of the material is considered. In other words, it ensures that the intermediate values that may appear can always be interpreted as the homogenization of some micro-structure. More importantly, the interpolation is based on the topological derivative concept. In fact, when a small perturbation of the density is considered either on the material ($\rho = 1$) or the void ($\rho = 0$), we recover the topological derivative change of the topology, this is adding an infinite circular insertion of the other material.

For macroscopic problems, a similar interpolation was firstly studied in [Amstutz, 2011b] and generalized for any Poisson ratio and proved to be in between the HS bound in [Ferrer, 2019]. For all these reasons, we use the SIMP-ALL interpolation method in this work, which is briefly presented in the following.

3.2.1. SIMP-ALL interpolation. In plane stress, the SIMP-ALL constitutive tensor is written in terms of the density variable as

$$\mathbb{C}(\rho) = 2\mu_{SA}(\rho)\mathbb{I} + [\kappa_{SA}(\rho) - \mu_{SA}(\rho)]I \otimes I \quad (21)$$

where the shear $\mu_{SA}(\rho)$ and bulk $\kappa_{SA}(\rho)$ parameters are defined by the following rational functions:

$$\mu_{SA}(\rho) = \frac{(\mu_1 - \mu_0)(\eta_{\mu_0} - \eta_{\mu_1})(1 - \rho)\rho + \mu_0(\mu_1 + \eta_{\mu_0})(1 - \rho) + \mu_1(\mu_0 + \eta_{\mu_1})\rho}{(\mu_1 + \eta_{\mu_0})(1 - \rho) + (\mu_0 + \eta_{\mu_1})\rho},$$

$$\kappa_{SA}(\rho) = \frac{(\kappa_1 - \kappa_0)(\eta_{\kappa_0} - \eta_{\kappa_1})(1 - \rho)\rho + \kappa_0(\kappa_1 + \eta_{\kappa_0})(1 - \rho) + \kappa_1(\kappa_0 + \eta_{\kappa_1})\rho}{(\kappa_1 + \eta_{\kappa_0})(1 - \rho) + (\kappa_0 + \eta_{\kappa_1})\rho}.$$

with $\eta_{\mu_0} = \frac{\kappa_0\mu_0}{2\mu_0 + \kappa_0}$, $\eta_{\mu_1} = \frac{\kappa_1\mu_1}{2\mu_1 + \kappa_1}$, $\eta_{\kappa_0} = \mu_0$, and $\eta_{\kappa_1} = \mu_1$. The parameters μ_1 , κ_1 and μ_0 , κ_0 stands for the shear and bulk modulus of the material and the void. We recall that the Young and Poisson ratio are related with the shear and bulk modulus in plane stress through $E = \frac{4\kappa\mu}{\kappa + \mu}$ and $\nu = \frac{\kappa - \mu}{\kappa + \mu}$.

3.2.2. SIMP-ALL relation with topological derivative. By construction, the SIMP-ALL interpolation coincides in the limits $\rho = 0$ and $\rho = 1$ with the constitutive

tensor \mathbb{C}_0 and \mathbb{C}_1 and its derivative with the topological derivative $d\mathbb{C}_0$ and $-d\mathbb{C}_1$. More specifically,

$$\begin{aligned} \mathbb{C}(0) &= \mathbb{C}_0 & \text{and} & & \mathbb{C}'(0) &= d\mathbb{C}_0 \\ \mathbb{C}(1) &= \mathbb{C}_1 & & & \mathbb{C}'(1) &= -d\mathbb{C}_1. \end{aligned} \quad (22)$$

Thus, the SIMP-ALL interpolation ensures that a small perturbation of the density in one of the two phases ($\rho = 0$ or $\rho = 1$) is equivalent to consider a material that its properties are obtained by computing the homogenization tensor of a microstructure made by one of these phases with circular insertions of the other phase.

3.2.3. SIMP-ALL interpolation interpreted as homogenized micro-structure. As described in [Hashin and Shtrikman, 1963], any isotropic constitutive tensor should fulfill the Hashin-Shtrikman (HS) bounds. Here, we recall the upper and lower HS bounds for the shear $\mu_{LB}(\rho), \mu_{UB}(\rho)$ and bulk $\kappa_{LB}(\rho), \kappa_{UB}(\rho)$ modulus

$$\begin{aligned} \mu_{LB}(\rho) &= \mu_0(1-\rho) + \mu_1\rho - \frac{(1-\rho)\rho(\mu_1 - \mu_0)^2}{\mu_0\rho + \mu_1(1-\rho) + \frac{\kappa_0\mu_0}{2\mu_0 + \kappa_0}}, \\ \mu_{UB}(\rho) &= \mu_0(1-\rho) + \mu_1\rho - \frac{(1-\rho)\rho(\mu_1 - \mu_0)^2}{\mu_0\rho + \mu_1(1-\rho) + \frac{\kappa_1\mu_1}{2\mu_1 + \kappa_1}}, \\ \kappa_{LB}(\rho) &= \kappa_0(1-\rho) + \kappa_1\rho - \frac{(1-\rho)\rho(\kappa_1 - \kappa_0)^2}{\kappa_0\rho + \kappa_1(1-\rho) + \mu_0}, \\ \kappa_{UB}(\rho) &= \kappa_0(1-\rho) + \kappa_1\rho - \frac{(1-\rho)\rho(\kappa_1 - \kappa_0)^2}{\kappa_0\rho + \kappa_1(1-\rho) + \mu_1}. \end{aligned}$$

We recall that in work [Ferrer, 2019], the proposed SIMP-ALL interpolation for the shear and the bulk modulus were proved to remain in between the HS bounds for any pair of materials at any value of the density. This is

$$\mu_{UB}(\rho) \geq \mu_{SA}(\rho) \geq \mu_{LB}(\rho) \quad \text{and} \quad \kappa_{UB}(\rho) \geq \kappa_{SA}(\rho) \geq \kappa_{LB}(\rho) \quad \forall \rho \in [0, 1]. \quad (23)$$

Thus, this important property implies that the *gray* regions $0 < \rho < 1$ that appear in the topologies during the optimization process when using the SIMP-ALL interpolation can always be understood as homogenized isotropic microstructure and not as a fictitious material.

3.2.4. Optimization problem. Let us now rewrite problem (19). Relaxing the characteristic function χ by its continuous counterpart ρ , the objective is:

$$\begin{aligned} \min_{\rho \in \mathcal{R}, w_{ij} \in \mathcal{V}} & \quad \|\mathbb{C}^h(\rho, w_{ij}) - \mathbb{C}^*\|_2 \\ \text{s.t.} & \quad (\varepsilon(\phi), \mathbb{C}(\rho) : \varepsilon(w_{ij})) + (\varepsilon(\phi), \mathbb{C}(\rho) : e_{ij}) = 0 \quad \forall \phi \in \mathcal{V}, \forall i, j \in [1, N] \end{aligned} \quad (24)$$

where $\mathbb{C}(\rho)$ corresponds to the SIMP-ALL constitutive tensor defined in (21). Note that here, we explicitly consider the cell problem as an equality constraint. The material design problem (24) is commonly called inverse homogenization problem [Nika and Constantinescu, 2019] and its relaxed version suffers from existence of minimizers [Allaire et al., 2002, Cherkaev, 2001]. A common solution in topology optimization problems is to add appropriate filters to the density [Bourdin, 2001] or to add a Perimeter functional. In this work, we use the second option.

4. USE OF PERIMETER FUNCTIONAL IN MATERIAL DESIGN

The main disadvantage of using the relaxed approach, in comparison with the level-set method, is that the final optimal topology may exhibit intermediate values and therefore no manufacturability of the topology is guaranteed. The more natural solution is to add a perimeter functional to the cost function that, apart from providing existence to the problem, penalizes the intermediate values of the density. Following work, [Amstutz and Van Goethem, 2012] and the recent work [Amstutz et al., 2021], we extend in this work the use of the perimeter functional to the material design problem.

4.1. Perimeter functional definition. The relative perimeter functional of a domain $\Omega \subset Y$ is defined as

$$\text{Per}(\Omega) = \int_{\partial\Omega \setminus (\partial Y \cap \partial\Omega)} dx.$$

In general, this functional is not Fréchet differentiable and thus gradient-based optimizers cannot be used. However, due to the Γ -convergence theory, the functional may be approximated by a sequence of differentiable functional $\text{Per}_\epsilon(\rho)$. The most renowned approximation is the Modica-Mortola [Modica and Mortola, 1977] type of functional, however in this work, we prefer to use the type of functional presented in [Amstutz and Van Goethem, 2012] and [Amstutz et al., 2021] since the periodic condition of the micro-structure can be easily tackled. To this aim, we define the approximated periodic perimeter as

$$\text{Per}_\epsilon(\rho) = \frac{1}{\epsilon} \int_D (1 - L_\epsilon(\rho)) \rho \, dx \quad (25)$$

where the linear operator $L_\epsilon : L^\infty_\#(Y, [0, 1]) \rightarrow L^2_\#(Y, [0, 1])$ is the solution of the following problem

$$\begin{cases} -\epsilon^2 \Delta \rho_\epsilon + \rho_\epsilon = \rho & \text{in } Y \\ y \mapsto \rho_\epsilon(y) & Y - \text{periodic.} \end{cases} \quad (26)$$

By imposing periodicity to $\rho_\epsilon = L_\epsilon(\rho)$, the periodic perimeter (25) extends the results of the relative perimeter [Amstutz and Van Goethem, 2012] and total perimeter [Amstutz et al., 2021] where Neumann and Robin conditions were imposed in the elliptic problem (26).

4.2. Manufacturable material design problem. The use of the periodic Perimeter in the material design problem will force a final periodic topology with a clear interface and therefore manufacturable. For this reason, we will call the manufacturable material design problem to the following optimization problem

$$\begin{aligned} \min_{\rho \in \mathcal{R}, w_{ij} \in \mathcal{V}} \quad & \|\mathbb{C}^h(\rho, w_{ij}) - \mathbb{C}^*\|_p + \alpha \text{Per}_\epsilon(\rho) \\ \text{s.t.} \quad & (\varepsilon(\phi), \mathbb{C}(\rho) : \varepsilon(w_{ij})) + (\varepsilon(\phi), \mathbb{C}(\rho) : e_{ij}) = 0 \quad \forall \phi \in \mathcal{V}, \forall i, j \in [1, N] \end{aligned} \quad (27)$$

where the homogenized constitutive tensor, already defined in (5), can be written as

$$\mathbb{C}_{ijkl}^h = (e_{ij} + \varepsilon(w_{ij}), \mathbb{C}(\rho) : (e_{kl} + \varepsilon(w_{kl}))). \quad (28)$$

Note that the parameter α plays will be selected depending on the optimization problem. The manufacturable material design problem will be solved by a sequence of optimization problems with decreasing ϵ values. The optimal topology of each

optimization problem will be used as an initial guess for the upcoming one. Note also that the Perimeter functional value increase as ϵ decreases, thus the influence of the perimeter functional will be more remarkable in the last optimization problems. We will start with a large value of ϵ (of order $|Y|$) and will be decreased up to the size of the mesh h . This choice of the ϵ sequence leads to an optimization strategy that focuses on minimizing the distance term in the first optimization problems and decreasing the perimeter in the last optimization problems. Thus, finding first a topology similar to the target one and then making it manufacturable. Starting already from small values of ϵ would constraint unnecessarily the optimization problem and favor topologies that are very close to the initial guess. Note that other constraints, like minimum length or volume constraints, can be added to problem (27) and handled with an augmented Lagrangian scheme [Amstutz, 2011a] or a null-space optimization algorithm [Feppon et al., 2020].

4.2.1. *Reduced formulation.* Since problem (27) corresponds to a PDE-constrained optimization problem, we will use in this work its reduced formulation [Tröltzsch, 2010]. This is,

$$\min_{\rho \in \mathcal{R}} \|\mathbb{C}^h(\rho, w_i(\rho)) - \mathbb{C}^*\|_p + \alpha \text{Per}_\epsilon(\rho), \quad (29)$$

where $\mathbb{C}^h(\rho, w_i(\rho))$ is defined in (28) with $w_i(\rho)$ the solutions of the equilibrium $(\varepsilon(\phi), \mathbb{C} : \varepsilon(w_j)) + (\varepsilon(\phi), \mathbb{C} : e_j) = 0$. Note that the reduced formulation considers w_i not as a design variable but as a function depending implicitly of ρ through the equilibrium equation. This is possible due to the unique solution of the cell problem. Thus, the problem will be written as

$$\min_{\rho \in \mathcal{R}} J(\rho, w_i(\rho)) = F(\rho, w_i(\rho)) + \alpha \text{Per}_\epsilon(\rho), \quad (30)$$

where the distance functional is defined as

$$F(\rho, w_i(\rho)) = \|\mathbb{C}^h(\rho, w_i(\rho)) - \mathbb{C}^*\|_2 = \left(\sum_{ij} (\mathbb{C}_{ij}^h(\rho, w_i) - \mathbb{C}_{ij}^*)^2 \right)^{1/2}.$$

4.2.2. *Computation of the gradient in L^2 .* Since the problem is now Fréchet differentiable, the directional derivative of the distance functional F at $\rho \in \mathcal{R}$ in the direction $\tilde{\rho} \in \mathcal{R}$ can be obtained as

$$\begin{aligned} DF(\rho, w_i(\rho))\tilde{\rho} &= 1/2 \left(\sum_{ij} (\mathbb{C}_{ij}^h(\rho, w_i) - \mathbb{C}_{ij}^*)^2 \right)^{-1/2} 2 \left(\sum_{ij} \mathbb{C}_{ij}^h(\rho, w_i) - \mathbb{C}_{ij}^* \right) D\mathbb{C}_{ij}^h(\rho, w_i(\rho))\tilde{\rho} \\ &= F(\rho, w_i(\rho))^{-1} \sum_{ij} (\mathbb{C}_{ij}^h(\rho, w_i) - \mathbb{C}_{ij}^*) D\mathbb{C}_{ij}^h(\rho, w_i(\rho))\tilde{\rho}. \end{aligned} \quad (31)$$

As presented in Appendix A, the directional derivative of the homogenized constitutive tensor reads as

$$D\mathbb{C}_{ij}^h(\rho, w_i(\rho))\tilde{\rho} = \int_Y (e_{ij} + \varepsilon(w_{ij})) : \mathbb{C}'(\rho) : (e_{kl} + \varepsilon(w_{kl})) \tilde{\rho} dy, \quad (32)$$

and therefore from the definition in $L^2(Y)$ of the gradient $D\mathbb{C}_{ij}^h(\rho, w_i(\rho))\tilde{\rho} = \int_D g \tilde{\rho}$, we obtain the gradient of the distance term g_F as

$$g_F(\rho) = F(\rho, w_i(\rho))^{-1} (\mathbb{C}_{ij}^h(\rho, w_i) - \mathbb{C}_{ij}^*) [(\varepsilon(w_i) + e_i) : \mathbb{C}'_h(\rho) : (\varepsilon(w_i) + e_i)].$$

10 INVERSE HOMOGENIZATION USING THE TOPOLOGICAL DERIVATIVE

Regarding the Perimeter term, the gradient can be directly computed from (25) by

$$\begin{aligned} D\text{Per}(\rho)\tilde{\rho} &= \frac{1}{\epsilon} \int_Y -L_\epsilon(\tilde{\rho})\rho + [1 - L_\epsilon(\rho)]\tilde{\rho} = \frac{1}{\epsilon} \int_Y -L_\epsilon^*(\rho)\tilde{\rho} + [1 - L_\epsilon(\rho)]\tilde{\rho} \, dx \\ &= \frac{1}{\epsilon} \int_Y [1 - 2L_\epsilon(\rho)]\tilde{\rho} \, dx, \end{aligned} \quad (33)$$

where we have used the self-adjoint property of the L_ϵ operator ($L_\epsilon = L_\epsilon^*$). By imposing the gradient definition in $L^2(Y)$ as $D\text{Per}(\rho)\tilde{\rho} = \int_D g_P \tilde{\rho} \, dx$ we have

$$g_P(\rho) = \frac{1}{\epsilon} (1 - 2L_\epsilon(\rho)).$$

Thus, the whole gradient is finally obtained as

$$g(\rho) = g_F(\rho) + \alpha g_P(\rho). \quad (34)$$

4.2.3. *Computation of the gradient in H^1 .* Since the gradient can be defined with other scalar product, we choose in this work the H^1 scalar product which allow us to select the amount of regularity of the gradient. Thus, the gradient g is the solution of

$$\epsilon^2 \int_D \nabla \phi \nabla g + \int_D \phi g = D\mathbb{C}_{ij}^h(\rho, w_i(\rho))\tilde{\rho} + \alpha D\text{Per}(\rho)\tilde{\rho}, \quad (35)$$

with $D\mathbb{C}_{ij}^h(\rho, w_i(\rho))\tilde{\rho}$ and $D\text{Per}(\rho)\tilde{\rho}$ defined in (32) and (33). Note that this choice of scalar product acts a filtering technique.

5. NUMERICAL RESULTS

Let's now solve the manufacturable material design problem. Our experience is that in general the problem may present many local minima and therefore there is a strong influence on the initial guess. Another key factor for finding a convenient solution is the choice of the norm in (29). For simplicity, we have chosen an L^2 norm for measuring the error. However, more sophisticated norms could be chosen. For example larger L^p norms or a weighted norm through a positive definite matrix. Of course, the proper choice for each application is left to the material designer.

5.1. **Optimization algorithm.** As mentioned above, problem (29) is now differentiable and thus gradient-based algorithms may be used. In this work, we use a simple but effective projected gradient method to deal with the box constraints for a fixed ϵ value. To ensure that the projected gradient direction is descending the cost, we use an adaptive line search method, see Algorithm 1. More specifically, in this work we have taken $\eta = 3$ and $\beta = 0.05$ in order to have a fast convergence but controlling at the same time the change of the topology at each iteration. Regarding the L_ϵ of the perimeter functional, in practice, we compute a Cholesky decomposition when starting the ϵ loop to efficiently solve the discretization of the weak version of (26). In all the examples, we use an structured mesh in the domain $Y = \{(y_1, y_2) \mid 0 < y_1, y_2 < 1\}$ of 40x40 quadrilaterals subdivided in 4 triangles leading to a total of 6400 \mathbb{P}_1 elements. We take for the Young modulus and Poisson ratio of the material $E_1 = 1$, $\nu_1 = 1/3$ and the void $E_0 = 10^{-3}$, $\nu_0 = 1/3$. We recall that the bulk and shear parameters in plane stress are obtained as $\mu = \frac{E}{2(1+\nu)}$ and $\kappa = \frac{E}{2(1-\nu)}$

Algorithm 1 Projected gradient algorithm

```

1: Choose  $\rho_0$  and compute  $J_0 = J(\rho_0)$  and  $g_0 = g(\rho_0)$  from (30) and (34)
2: Take  $\epsilon = |Y|$  and  $\tau = \|\rho_0\|_2/\|g_0\|_2$ 
3: while  $\epsilon > h$  do
4:   while  $\|\rho_{k+1} - \rho_k\|_2 > \text{TOL}$  do
5:     while  $|J_{k+1} - J_k| > 0$  and  $\|\rho_{k+1} - \rho_k\|_2 > \beta\|\rho_k\|_2$  do
6:        $\rho_{k+1} = \max(0, \min(1, \rho_k - \tau g(\rho_k)))$ 
7:       Compute  $J_{k+1} = J(\rho_{k+1})$  and  $g_{k+1} = g(\rho_{k+1})$  from (30) and (34)
8:        $\tau \leftarrow \tau/2$ 
9:     end while
10:    Take  $\tau \leftarrow \eta\tau$  and  $k \leftarrow k + 1$ 
11:   end while
12:    $\epsilon \leftarrow \epsilon/2$ 
13: end while

```

5.2. Example 1. Rank-1 laminate. The first example to solve is the rank-1 laminate case. The target \mathbb{C}^* is computed from the homogenized constitutive tensor \mathbb{C}^h of a microstructure full of material with a centered horizontal rectangular void of 0.4 width. The initial guess is a full material cell with a centered circle void of radius $r = 0.8$. Since no intermediate materials tend to appear in the final topology, we take in this case $\alpha = 0$ and thus the Perimeter term and ϵ loop is not considered. In Figure 1, we show the evolution of the cost (in blue and logarithmic scale) and the volume $\text{Vol}(\rho) = \int_D \rho \, dx$ (in red) during the iterations. We also show the constitutive tensor for the target and the optimal designs. We observe the monotone decrease of the difference between the constitutive tensors during the iterations and the proximity of the optimal $\mathbb{C}(\rho^*)$ with the target constitutive tensor \mathbb{C}^* . In the last row of Figure 1, we also show the design variable during the iterations and we observe that although no gray areas appear in the initial and final topologies, the optimization path is taking profit, in contrast with level-set methods, of intermediate values.

5.3. Example 2. Circular hole. In this second example, the \mathbb{C}^* is obtained by computing the homogenized constitutive tensor \mathbb{C}^h of a square full microstructure with a centered circular void inclusion of radius $r = 0.4$. Both the topology and the constitutive target tensor \mathbb{C}^* are shown in Figure 2. We consider the same topology of the last example as an initial guess, this is a square full microstructure with a centered circular void inclusion of radius $r = 0.8$. This problem in the shape optimization context would be easily solved by decreasing the radius of the inclusion. However, it is not straightforward when considering the relaxation of the problem. In fact, when $\alpha = 0$ we observe that the constitutive tensor significantly decreases during iterations, see the red line in the upper-left image of Figure 2. However, the local minimum obtained exhibits large regions of gray areas. The optimization process had tried to fill the circular hole with intermediate values. See the increase of volume during the iterations in the lower-left image of Figure 2 (red line). Although the optimal constitutive tensor is close to the target one and the optimal microstructure may be physically understood (due to the SIMP-ALL interpolation), the optimal micro-structure is not manufacturable. Thus we also compute the example with $\alpha = 0.1$ and we observe in Figure 2 that although the optimization process is

12 INVERSE HOMOGENIZATION USING THE TOPOLOGICAL DERIVATIVE

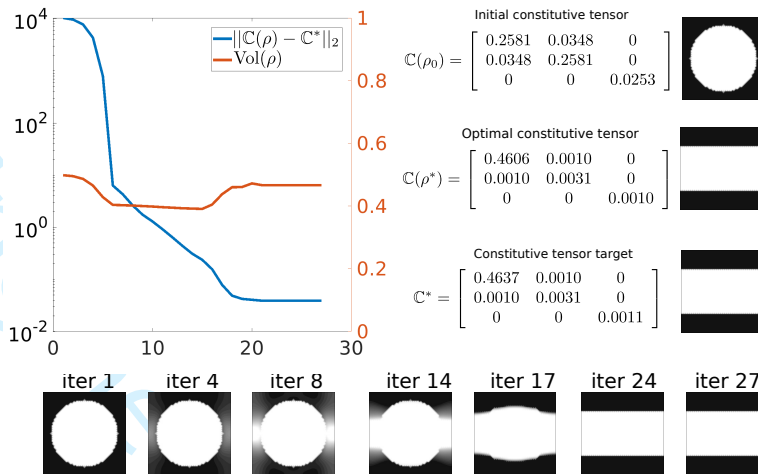


FIGURE 1. The topological derivative is used in a relaxed approach to find an optimal topology that has a homogenized constitutive tensor \mathbb{C}^h close to the target one \mathbb{C}^* . In contrast with level-set methods, the optimization process take profit of the intermediate values of the design variable.

similar at the first iterations, in this second case the optimal topology exhibits a clear interface. In general, when the Perimeter term starts being relevant (ϵ small), there is no guarantee that the difference of the constitutive tensor with the target one decreases. However, for this case, the difference between constitutive tensor also decrease (not monotonically) when the Perimeter term starts being relevant.

In contrast to the $\alpha = 0$ case, we observe in the upper-right image of Figure 2 how the approximated perimeter decreases for small values of ϵ when $\alpha = 0.1$. The final topology for $\alpha = 0.1$ is now manufacturable due to the Perimeter term. We also observe the proximity of the optimal constitutive tensor with the target constitutive tensor. In the last row, we show the iterations of the topology during the iterations. We observe similar optimization paths of both cases until the perimeter terms become relevant and remove the gray areas in the $\alpha = 0.1$ case. We have also plotted the volume and the variation of ϵ/h to better describe the optimization process.

Note that using the Perimeter will not necessarily decrease the distance potential, its intent is to provide manufacturable topologies. Of course, if the target topology has been obtained as the homogenization of some manufacturable topology (as we do in this work), then the perimeter may help in removing the local minimum that presents gray areas.

5.4. Example 3. Negative Poisson ratio. We end this work with a more challenging example. The objective is to find a material that presents a fictitious negative Poisson ratio (not necessarily isotropic). To do so, we first follow the work of [Amstutz et al., 2010] where the objective is to minimize

$$J(\chi) = \frac{\psi_a : (\mathbb{C}^h(\chi))^{-1} : \psi_b}{\psi_a : (\mathbb{C}^h(\chi))^{-1} : \psi_a} + \frac{\psi_b : (\mathbb{C}^h(\chi))^{-1} : \psi_a}{\psi_b : (\mathbb{C}^h(\chi))^{-1} : \psi_b} \quad (36)$$

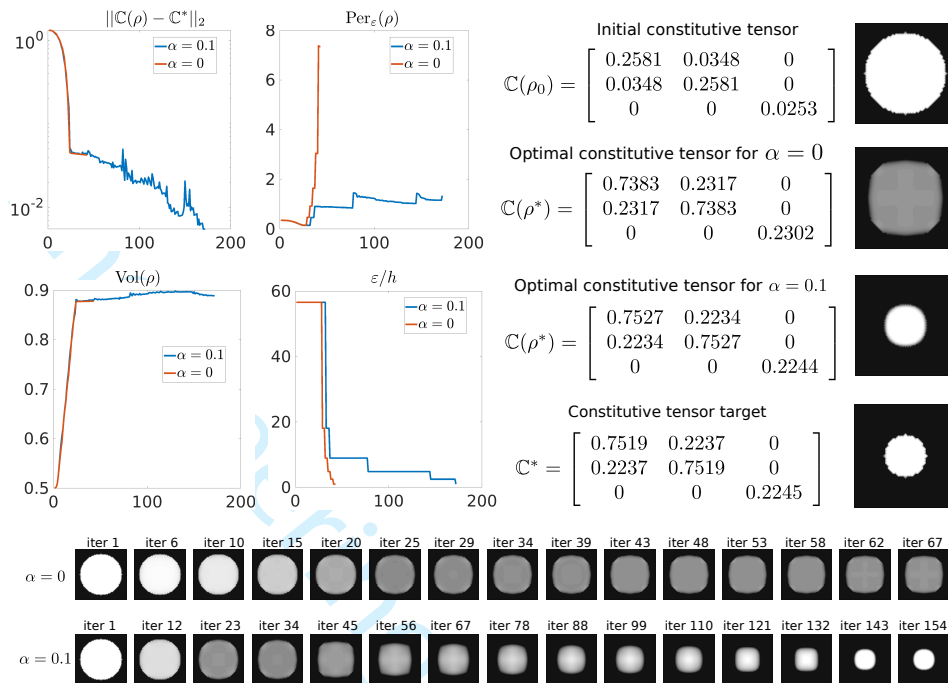


FIGURE 2. Using the topological derivative in a relaxed formulation may lead to topologies with large gray areas ($\alpha = 0$). Adding the Perimeter term $Per_\varepsilon(\rho)$ ($\alpha = 0.1$) enables to obtain manufacturable (clear interface) and satisfactory designs in terms of $\|\mathbb{C}(\rho^*) - \mathbb{C}^*\|$.

with $\psi_a = [1 \ 0 \ 0]$ and $\psi_b = [0 \ 1 \ 0]$ by the methodology proposed in [Amstutz et al., 2010] (level-set and fix-point algorithm) as explained in Section 3.1 and we obtain the target constitutive tensor as homogenized constitutive tensor \mathbb{C}^h of the optimal topology obtained when solving problem (36) with the level-set method. We show both the target constitutive tensor and its corresponding topology in Figure 3. Once we have obtained \mathbb{C}^* we solve the problem directly with $\alpha = 0$ since in this case, the optimal topology presents no intermediate values.

We show the constitutive tensor difference during the iterations and the change of volume. In this case, we consider a full square domain with 24 homogeneously distributed small holes of radius $r = 1/12$. We show the topology (repeated 4 times) and its constitutive homogenized tensor in Figure 3. We also show the optimal constitutive tensor and its corresponding topology.

We observe a large decrease in the cost function even if the initial guess was far from the target. Although it is not explicitly required in optimization problem, we also see that the optimal topology is very similar. In the last row of Figure 3, we show the optimization path and how the proposed regularized methodology takes profit of using intermediate values. This type of optimization path could not be obtained through the topological derivative (or shape derivative) in the level-set function approach described in Section 3.1. Finally, our experience is that this last example is complex and challenging, and a satisfactory minimum may only be obtained if proper and specific initial guesses are considered.

14

INVERSE HOMOGENIZATION USING THE TOPOLOGICAL DERIVATIVE

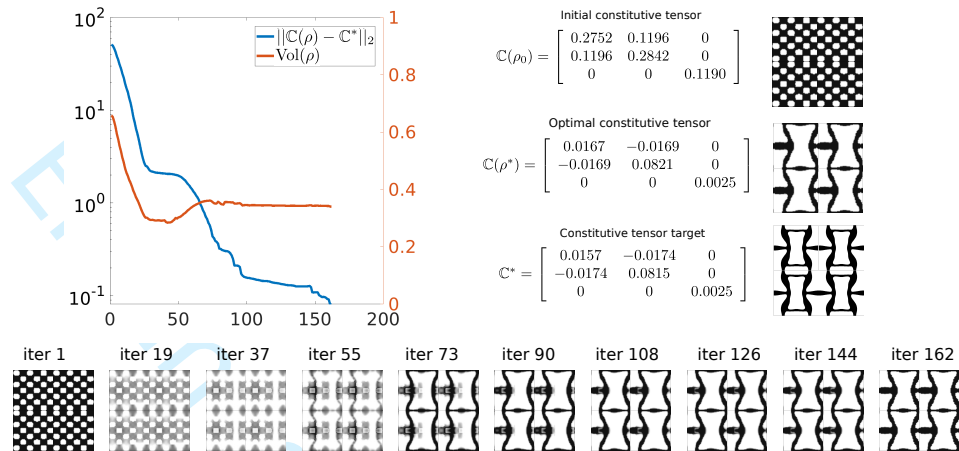


FIGURE 3. *The challenging problem of finding a negative Poisson ratio is solved with the use of the topological derivative in a relaxed formulation. The problem directly find manufacturable solution so no Perimeter term is added ($\alpha = 0$). In this case, the solution is not only close to the target topology in terms of the constitutive tensor but also in terms of topology.*

6. FINAL REMARKS

In this work, we proposed a new methodology for solving the inverse homogenization problem with the use of topological derivative.

The proposed relaxation approach in conjunction with the SIMP-ALL interpolation have show to be effective for solving the inverse homogenization approach. On the one hand, we were able to use classical optimization algorithms like the projected gradient method. On the other side, the optimization procedure ends successfully by reaching the target constitutive behavior C^* . Additionally, we have seen that the perimeter functional remove intermediate values and provide manufacturable topologies (with clear interfaces). We also observed that the combination of first minimizing the distance functional and then the perimeter term is a convenient strategy to obtain satisfying solutions. Regarding the optimization side, the success of using a projected gradient for solving this problem opens the possibility of using many other optimizers and optimization packages. In addition, we have shown that the path to obtain optimal topologies is very different to the level-set approach. Through intermediate gray topologies, this approach provides a new way to obtain optimal topologies when using the topological derivative. Finally, we may also conclude that the inverse homogenization problem is hard to solve and the solution is full of local minima. We experienced the importance of the initial guess in the final solution. The high number of local minima that could appear when solving the problem is not due to the topological derivative aspects but to the proposed relaxed formulation, which explores not only classical topologies but also homogenized structures. The disadvantage is that many local minima may appear, the advantage is that with a proper initial guess, satisfactory solutions might often be obtained. We left the optimization of the microstructures boundary shapes and 3D examples for future work.

APPENDIX A. DIRECTIONAL DERIVATIVE OF THE HOMOGENIZED CONSTITUTIVE TENSOR

In this appendix, we compute the directional derivative of the homogenized constitutive tensor

$$\mathbb{C}_{ijkl}^h(\rho, w(\rho)) = (e_{ij}, \mathbb{C}(\rho) : e_{kl}) + (e_{ij}, \mathbb{C}(\rho) : \varepsilon(w_{kl})). \quad (37)$$

The directional derivative of the homogenized constitutive tensor at $\rho \in \mathcal{R}$ in the direction $\tilde{\rho} \in \mathcal{R}$ reads as

$$D_{\rho} \mathbb{C}_{ijkl}^h(\rho, w(\rho)) \tilde{\rho} = D_{\rho} \mathbb{C}_{ijkl}^h \tilde{\rho} + (D_w \mathbb{C}_{ijkl}^h)(D_{\rho} w(\tilde{\rho}))$$

The first term can be directly computed by deriving (37) as

$$D_{\rho} \mathbb{C}_{ijkl}^h \tilde{\rho} = (e_{ij}, d\mathbb{C} : e_{kl}) + (e_{ij}, d\mathbb{C} : \varepsilon(w_{kl}))$$

where $d\mathbb{C} = \mathbb{C}'(\rho) \tilde{\rho}$. For the second term, defining $\tilde{w}_{kl} = D_{\rho} w(\tilde{\rho})$ we have

$$(D_w \mathbb{C}_{ijkl}^h)(D_{\rho} w(\tilde{\rho})) = D_w \mathbb{C}_{ijkl}^h \tilde{w}_{kl} = (e_{ij}, \mathbb{C}(\rho) : \varepsilon(\tilde{w}_{kl})).$$

Now, taking derivative in the equilibrium equations of the cell problem (3), we have

$$(\varepsilon(\phi), d\mathbb{C} : \varepsilon(w_{ij})) + (\varepsilon(\phi), \mathbb{C} : \varepsilon(\tilde{w}_{ij})) + (\varepsilon(\phi), d\mathbb{C} : e_{ij}) = 0 \quad \forall \phi \in \mathcal{V}.$$

Defining the adjoint field p as the solution of

$$(\varepsilon(\tilde{w}_{kl}), \mathbb{C}(\rho) : \varepsilon(p)) = -D_w \mathbb{C}_{ijkl}^h \tilde{w}_{kl} = -(e_{ij}, \mathbb{C}(\rho) : \varepsilon(\tilde{w}_{kl}))$$

we observe from the equilibrium equation that the adjoint and state fields are equivalent $p = w_{ij}$. Using the self-adjoint property of the scalar product in L^2 , we have then

$$\begin{aligned} D_w \mathbb{C}_{ijkl}^h \tilde{w}_{kl} &= -(\varepsilon(\tilde{w}_{kl}), \mathbb{C} : \varepsilon(p)) = (\varepsilon(p), d\mathbb{C} : \varepsilon(w_{ij})) + (\varepsilon(p), d\mathbb{C} : e_{ij}) \\ &= (\varepsilon(w_{ij}), d\mathbb{C} : \varepsilon(w_{kl})) + (\varepsilon(w_{ij}), d\mathbb{C} : e_{kl}) \end{aligned} \quad (38)$$

Thus,

$$\begin{aligned} D_{\rho} \mathbb{C}_{ijkl}^h(\rho, w(\rho)) \tilde{\rho} &= (e_{ij}, d\mathbb{C} : e_{kl}) + (e_{ij}, d\mathbb{C} : \varepsilon(w_{kl})) + (\varepsilon(w_{ij}), d\mathbb{C} : \varepsilon(w_{kl})) + (\varepsilon(w_{ij}), d\mathbb{C} : e_{kl}) \\ &= (\varepsilon(w_{ij}) + e_{ij}, d\mathbb{C} : (\varepsilon(w_{kl}) + e_{kl})) \end{aligned} \quad (39)$$

and therefore

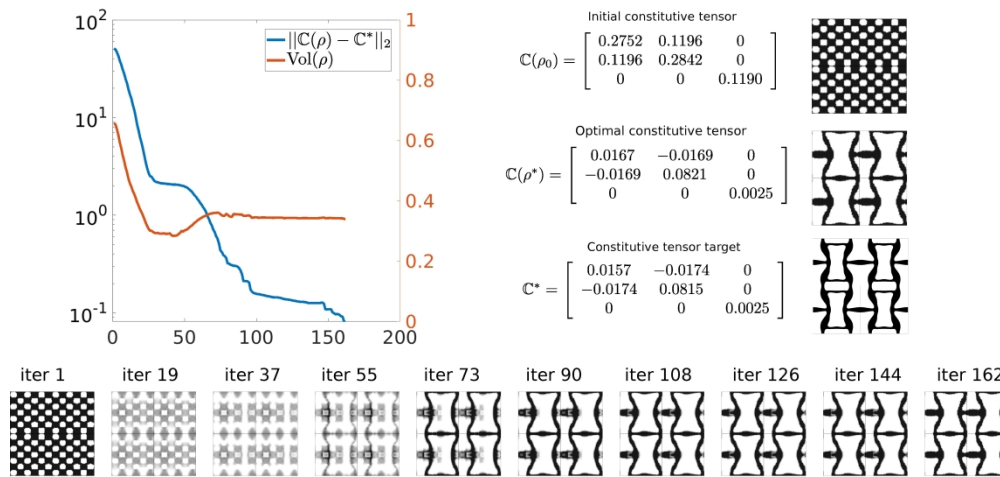
$$D_{\rho} \mathbb{C}_{ijkl}^h(\rho, w(\rho)) \tilde{\rho} = \int_Y (e_{ij} + \varepsilon(w_{ij})) : \mathbb{C}'(\rho) : (e_{kl} + \varepsilon(w_{kl})) \tilde{\rho} dy. \quad (40)$$

REFERENCES

- [Allaire, 2012] Allaire, G. (2012). *Shape optimization by the homogenization method*, volume 146. Springer Science & Business Media.
- [Allaire et al., 2002] Allaire, G., Jouve, F., and Toader, A.-M. (2002). A level-set method for shape optimization. *Comptes Rendus Mathématique*, 334(12):1125–1130.
- [Amstutz, 2011a] Amstutz, S. (2011a). Augmented lagrangian for cone constrained topology optimization. *Computational Optimization and Applications*, 49(1):101–122.
- [Amstutz, 2011b] Amstutz, S. (2011b). Connections between topological sensitivity analysis and material interpolation schemes in topology optimization. *Structural and Multidisciplinary Optimization*, 43(6):755–765.
- [Amstutz and Andrä, 2006] Amstutz, S. and Andrä, H. (2006). A new algorithm for topology optimization using a level-set method. *Journal of Computational Physics*, 216(2):573–588.
- [Amstutz et al., 2018] Amstutz, S., Dapogny, C., and Ferrer, Å. (2018). A consistent relaxation of optimal design problems for coupling shape and topological derivatives. *Numerische mathematik*, 140(1):35–94.

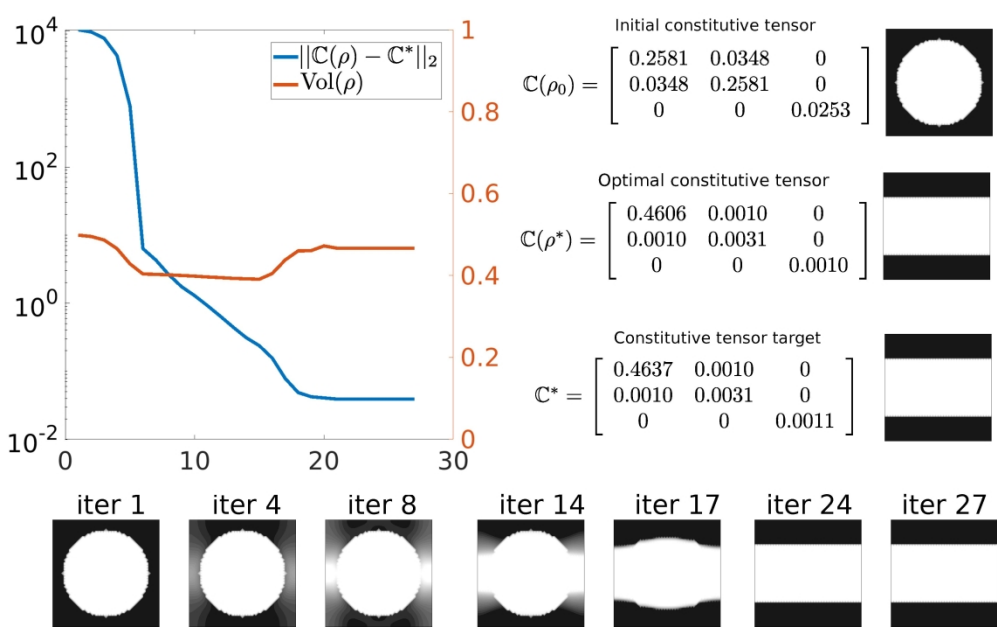
- [Amstutz et al., 2021] Amstutz, S., Dapogny, C., and Ferrer, A. (2021). A consistent approximation of the total perimeter functional for topology optimization algorithms. *submitted*.
- [Amstutz et al., 2010] Amstutz, S., Giusti, S., Novotny, A., and de Souza Neto, E. (2010). Topological derivative for multi-scale linear elasticity models applied to the synthesis of microstructures. *International Journal for Numerical Methods in Engineering*, 84(6):733–756.
- [Amstutz and Van Goethem, 2012] Amstutz, S. and Van Goethem, N. (2012). Topology optimization methods with gradient-free perimeter approximation. *Interfaces and Free Boundaries*, 14(3):401–430.
- [Bendsøe and Sigmund, 2003] Bendsøe, M. P. and Sigmund, O. (2003). *Topology optimization. Theory, methods and applications*. Springer-Verlag, Berlin.
- [Bourdin, 2001] Bourdin, B. (2001). Filters in topology optimization. *International journal for numerical methods in engineering*, 50(9):2143–2158.
- [Cherkaev, 2001] Cherkaev, E. (2001). Inverse homogenization for evaluation of effective properties of a mixture. *Inverse Problems*, 17(4):1203.
- [Feppon et al., 2020] Feppon, F., Allaire, G., and Dapogny, C. (2020). Null space gradient flows for constrained optimization with applications to shape optimization. *ESAIM: Control, Optimization and Calculus of Variations*, 26:90.
- [Ferrer, 2017] Ferrer, A. (2017). *Multi-scale Topological Design of Structural Materials: An Integrated Approach*. Ph.D. Thesis, Universitat Politècnica de Catalunya (UPC) - International Center for Numerical Methods in Engineering (CIMNE), Barcelona, Spain.
- [Ferrer, 2019] Ferrer, A. (2019). Simp-all: A generalized simp method based on the topological derivative concept. *International Journal for Numerical Methods in Engineering*, 120(3):361–381.
- [Ferrer et al., 2021] Ferrer, A., Geoffroy-Donders, P., and Allaire, G. (2021). Stress minimization for lattice structures. part i: Micro-structure design. *Philosophical Transactions of the Royal Society A*, 379(2201):20200109.
- [Giusti and Novotny, 2016] Giusti, S. M. and Novotny, A. A. (2016). *Multi-objective Topology Optimization Design of Micro-structures*, volume 49 of *Computational Modeling, Optimization and Manufacturing Simulation of Advanced Engineering Materials*, pages 21–47. Springer.
- [Giusti et al., 2010] Giusti, S. M., Novotny, A. A., and de Souza Neto, E. A. (2010). Sensitivity of the macroscopic response of elastic microstructures to the insertion of inclusions. *Proceeding of the Royal Society A: Mathematical, Physical and Engineering Sciences*, 466:1703–1723.
- [Hashin and Shtrikman, 1963] Hashin, Z. and Shtrikman, S. (1963). A variational approach to the theory of the elastic behaviour of multiphase materials. *Journal of the Mechanics and Physics of Solids*, 11(2):127–140.
- [Méndez et al., 2017] Méndez, C. G., Podestá, J. M., Lloberas-Valls, O., Toro, S., Huespe, A. E., and Oliver, J. (2017). Computational material design for acoustic cloaking. *International Journal for Numerical Methods in Engineering*, 112(10):1353–1380.
- [Modica and Mortola, 1977] Modica, L. and Mortola, S. (1977). Il limite nella;convergenza di una famiglia di funzionali ellittici, *boll. Math. Ital.*, A, 14.
- [Nika and Constantinescu, 2019] Nika, G. and Constantinescu, A. (2019). Design of multi-layer materials using inverse homogenization and a level set method. *Computer Methods in Applied Mechanics and Engineering*, 346:388–409.
- [Novotny and Sokolowski, 2013] Novotny, A. A. and Sokolowski, J. (2013). *Topological derivatives in shape optimization*. Interaction of Mechanics and Mathematics. Springer-Verlag, Berlin, Heidelberg.
- [Podestá et al., 2019] Podestá, J. M., Méndez, C. M., Toro, S., and Huespe, A. E. (2019). Symmetry considerations for topology design in the elastic inverse homogenization problem. *Journal of the Mechanics and Physics of Solids*, 128:54–78.
- [Rossi et al., 2021] Rossi, N., Podestá, J. M., Bre, F., Méndez, C. G., and Huespe, A. E. (2021). A microarchitecture design methodology to achieve extreme isotropic elastic properties of composites based on crystal symmetries. *Structural and Multidisciplinary Optimization*, 63:2459–2472.
- [R.Yera et al., 2020] R.Yera, N.Rossi, C.G.Méndez, and A.E.Huespe (2020). Topology design of 2d and 3d elastic material microarchitectures with crystal symmetries displaying isotropic properties close to their theoretical limits. *Applied Material Today*, 18:100456.
- [Sigmund, 1994] Sigmund, O. (1994). Materials with prescribed constitutive parameters: an inverse homogenization problem. *International Journal of Solids and Structures*, 31(17):2313–2329.

- [Sigmund, 1995] Sigmund, O. (1995). Tailoring materials with prescribed elastic properties. *Mechanics of Materials*, 20(4):351–368.
- [Tröltzsch, 2010] Tröltzsch, F. (2010). *Optimal control of partial differential equations: theory, methods, and applications*, volume 112. American Mathematical Soc.
- [Vermaak et al., 2019] Vermaak, N., Michailidis, G., Faure, A., Parry, G., Estevez, R., Jouve, F., Allaire, G., and Bréchet, Y. (2019). *Topological Optimization with Interfaces*, volume 282 of *Architected Materials in Nature and Engineering in Springer Series in Materials Science*, pages 173–193. Springer.

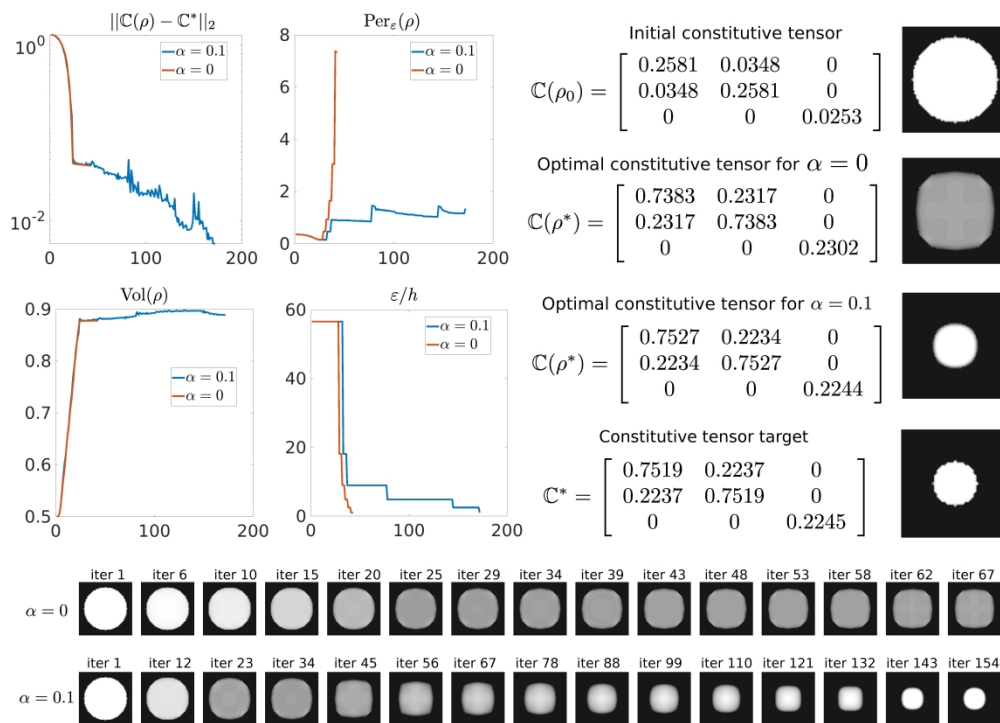


249x120mm (600 x 600 DPI)

1
2
3
4
5
6
7
8
9
10
11
12
13
14
15
16
17
18
19
20
21
22
23
24
25
26
27
28
29
30
31
32
33
34
35
36
37
38
39
40
41
42
43
44
45
46
47
48
49
50
51
52
53
54
55
56
57
58
59
60



184x116mm (600 x 600 DPI)



370x263mm (600 x 600 DPI)

•

References

- [1] Samuel Amstutz. Augmented lagrangian for cone constrained topology optimization. *Computational Optimization and Applications*, 49(1):101–122, 2011.
- [2] Florian Feppon, Grégoire Allaire, and Charles Dapogny. Null space gradient flows for constrained optimization with applications to shape optimization. *ESAIM: Control, Optimisation and Calculus of Variations*, 26:90, 2020.